Dye−Host Interactions for Local Effects Recognition in Homogeneous and Nanostructured Media

T. M. R. Viseu,* G. Hungerford, A. F. Coelho, and M. I. C. Ferreira

Centro de Física, Instituto de Materiais, 4710-057 Braga, Portugal

Received: February 28, 2003; In Final Form: June 24, 2003

Steady-state absorption and emission as well as time-resolved fluorescence spectra of NR (nile red) and ZnP (zinc tetraphenylporphyrin) were studied in a variety of solvents. All spectra were decomposed as a sum of Gaussian bands, and the spectral shifts found were analyzed in terms of the general solvatochromic theory. Ground state permanent dipoles, electronic spectra, and Onsager cavity radii were obtained for each dye in several solvents using intermediate neglect of differential overlap (INDO) software provided by ArgusLab. ZnP emission spectra also reveal the presence of a new band interpreted as due to an excitonic coupling between pairs of weakly interacting ZnP molecules. The center to center distance in these excitonic pairs was estimated. Studies were extended to the system ZnP−PVP (PVP refers to poly(vinylpyridine)), and its photophysical properties were determined. NR and ZnP were also incorporated into rigid matrixes of PS (polystyrene), PVP, SiO_2, and TiO_2. NR in these rigid media probes local polarities and enables the estimation of the effective dielectric constant of the matrixes. The behavior of ZnP emission when incorporated in the same rigid media was also analyzed. In particular, in PS and TiO_2 matrixes, the spectra were interpreted as the result of an excitonic coupling between pairs of porphyrin molecules and according to Kasha's theory the center to center distance between the interacting molecules could be estimated. The ZnP−SiO_2 emission spectrum is ascribed to monomeric porphyrin, while in the ZnP−PVP matrix the emission spectrum was interpreted in terms of two distinct emitting states.

1. Introduction

The sensitivity of fluorescence emission from molecules to the polarity of their environment has been recognized as an important means to probe local field effects either in homogeneous systems[1−4] or in heterogeneous systems such as micelles, vesicles, microemulsions[5,6] and sol−gel derived matrixes[7,8] or polymers.[9] Lately the application of photoluminescence methods to biology, biomedical and medical sciences[10] has become an expanding field. In fact progress has been recently reported in the field of fluorescence lifetime imaging measurement (FLIM).[11,12] The full understanding of many in vivo systems requires a deep knowledge of the photophysical properties of the naturally emitting species, in the case of autofluorescence studies[13] or else the design of appropriate fluorophores for incorporation in the systems under scrutiny.[14] Local field effects and restricted geometry are important parameters for the full understanding of such complex systems.[15] In many applications the fluorescent molecule probes simultaneously the local polarity of the host medium, specific chemical interactions, and geometrical or morphological constraints.[16]

In the present work, the authors have attempted to develop a unified methodology that would hopefully account for local effects in nanostructured media. In such media, the presence of voids of different sizes and shapes, the chemical disorder of the matrix, and the presence of adsorbed water molecules are examples that account for the diversity of local effects that are to be expected when dye−host interactions are examined.

To develop such a method nile red (NR) was chosen because of its well-known behavior as a solvatochromic probe, and it was therefore a suitable molecule to probe local polarities.[5,9,17] However, the methodology presented only becomes relevant if applicable to a wide range of host molecules, in particular to significantly less polar molecules than NR. For such reasons, the authors have chosen ZnTPP as a suitable model molecule, due to its intrinsic low polarity, associated with other interesting features such as aggregation effects and low quantum yield of fluorescence. Steady-state and time-resolved fluorescence of nile red and zinc tetraphenylporphyrin were examined in several solvents with a wide range of polarities. The work was further extended to the study of the spectroscopical and photophysical properties of the same dyes incorporated into SiO_2, TiO_2, polystyrene, and poly(4-vinylpyridine) matrixes.

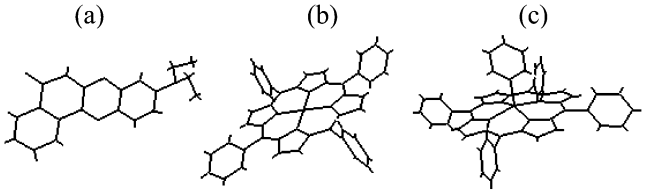

Figure 1. PM3 optimized structures for (a) nile red, (b) ZnP, and (c) ZnP−Py.

2. Experimental Section

Nile red (NR) and zinc *meso*-tetraphenylporphyrin (ZnP) were purchased from Aldrich Chemical Co. Inc and Porphyrin Products, respectively, and used without further purification. Polystyrene (PS) and poly(4-vinylpyridine) (PVP) were supplied by Aldrich Chemical Co. Inc. and used as received. All solvents were of spectroscopic grade. The molecular structures of NR, ZnP, and ZnP covalently linked to one pyridine unit (ZnP−Py) are given in Figure 1.

10.1021/jp030284k CCC: $25.00
Published on Web 11/11/2003

SiO_2 and TiO_2 matrixes were prepared by an acid-catalyzed sol−gel technique as previously described[7] and will be referred to as sg-SiO_2 and sg-TiO_2, respectively. TiO_2 samples were also prepared by reactive magnetron sputtering in a commercial Alcatel System, model SCM 650, under preparation conditions already described;[18] such samples will be referred to as sp-TiO_2. These matrixes were prepared as thin films deposited onto glass slides. The dyes were then incorporated by dipping each film into the appropriate stock solution. After dipping, each sample was gently washed with the solvent used, then allowed to dry for several days and finally cleaned with a soft tissue. Although an average concentration of the dye in the matrix (in the range $10^{-5}-10^{-3}$ M) can be obtained from the optical density of each film, the effective local concentration of the dye within the nanopores, expected to be significantly higher than the average,[19] cannot be accessed directly from the spectroscopical and photophysical data.

NR−PS, NR−PVP, ZnP−PS, and ZnP−PVP films were prepared by dipping glass slides into stock solutions of each dye and PS in benzene or PVP in chloroform. The films were allowed to dry for several days until a constant transmittance spectrum was measured.

Absorption and transmittance spectra were measured on a Shimadzu 3101 PC. The optical constants of each film were determined from the detailed analysis of the transmittance spectra in the range 250−2200 nm, by means of the Abèles matricial model, according to a previously reported methodology.[20] The effective refractive index and the void fraction of each matrix were determined by considering the measured complex refractive index as the result of multiple light scattering events within the nanostructured media, in agreement with the theory developed by Webman et al.[21]

The absorption spectrum of NR or ZnP in each of the films was obtained by considering the optical dispersion attributed to each dye in the 350−700 nm region to arise from electronic transitions between two molecular states, either $S_0 \rightarrow S_2$ or $S_0 \rightarrow S_1$.[20]

Fluorescence and excitation spectra were recorded on a Spex Fluorolog. Emission spectra of the films were measured in the front face optical arrangement in order to minimize self-absorption effects. Fluorescence quantum yields, ϕ_F, in solution were determined relative to either zinc tetraphenylporphyrin or rhodamine 6G, in ethanol. Determination of ϕ_F of the doped films was obtained relative to a dry sample of rhodamine 6G incorporated in a SiO_2 matrix.[22] Corrections were made by considering the effective refractive index of each matrix as previously reported.[20] Emission spectra for ϕ_F calculations were measured with excitation beam polarized vertically and emission beam observed at a viewing angle of 54.7° in order to correct for the effect of polarization on fluorescence intensity.

Fluorescence lifetimes were measured by means of a single-photon counting apparatus equipped with two types of excitation sources: (a) hydrogen-filled coaxial flash-lamp; (b) LED excitation sources with peak emissions at 495 and 560 nm, purchased from IBH (NanoLED). Cutoff filters were used to select the emission signal which was detected using a Hamamatsu R-2949 side-window photomultiplier. Data analysis was performed using software provided by IBH Consultants Ltd. Errors are given as three standard deviations and the contribution of each fluorescing component is expressed as a relative preexponential factor weighted by the lifetime in order to compare with steady-state data. All measurements were performed at room temperature.

An estimate of the ground-state permanent dipole moment of each dye and of the Onsager cavity radius of the solvents used throughout was obtained via a ZINDO calculation using ArgusLab 3.1 software (Planaria Software). This was a method developed by Zerner and co-workers[23,24] based on the intermediate neglect of differential overlap (INDO). The ZINDO calculation was performed on structures that had been geometrically optimized using a PM3 quantum mechanical model (also ArgusLab).

3. Solution Studies

Several authors[3,16,25] have established that general solvatochromic effects on the spectra are due to dispersive interactions and internal electric field effects. Accordingly, the observed solvatochromic shifts in the absorption and emission spectra, by reference to the vapor phase spectra are given, respectively, by

$$\Delta\bar{\nu}_{abs} = \bar{\nu}_{sol}^{abs} - \bar{\nu}_{vac}^{abs} = C_1 \frac{n^2-1}{2n^2+1} + C_2^{abs}\left(\frac{\epsilon-1}{\epsilon+2} - \frac{n^2-1}{n^2+2}\right) + C_3^{abs}\left(\frac{\epsilon-1}{\epsilon+2} - \frac{n^2-1}{n^2+2}\right)^2 \quad (1)$$

$$\Delta\bar{\nu}_{flu} = \bar{\nu}_{sol}^{flu} - \bar{\nu}_{vac}^{flu} = C_1 \frac{n^2-1}{2n^2+1} + C_2^{flu}\left(\frac{\epsilon-1}{\epsilon+2} - \frac{n^2-1}{n^2+2}\right) + C_3^{flu}\left(\frac{\epsilon-1}{\epsilon+2} - \frac{n^2-1}{n^2+2}\right)^2 \quad (2)$$

where $(n^2-1)/(2n^2+1) = f(n^2)$ refers to the redistribution of electrons, whereas the other two terms, $f(\epsilon, n^2)$ and $[f(\epsilon, n^2)]^2$, refer to the reorientation of dipoles. In many systems, such as when $C_1 > C_2$, the quadratic term may be neglected.[25] This is the case of the systems studied in this work, as will be shown.

By neglecting quadratic effects and combining eqs 1 and 2, we obtained the so-called Mataga−Lippert equation[25]

$$\Delta\bar{\nu}_{abs} - \Delta\bar{\nu}_{flu} = \frac{1}{4\pi\epsilon_0}\frac{2}{hc}\frac{\Delta\mu^2}{R^3}\left(\frac{\epsilon-1}{\epsilon+2} - \frac{n^2-1}{n^2+2}\right) \quad (3)$$

where $\Delta\mu = \mu_g - \mu_e$ is the difference in the dipole moment of the solute molecule between ground and excited states and R is the cavity radius considering the solute molecule a point dipole at the center of a spherical cavity immersed in the homogeneous solvent. ϵ is the static dielectric constant of the solvent and n the refractive index.

Very rarely such general effects are the only relevant dye−host interaction. There are well-known examples of the simultaneous occurrence of specific interactions, such as hydrogen bonding,[26] aggregation,[27,20]and chemical bonding.[28] In addition, it has also been found by some authors, such as Maroncelli and Fleming[4] and S. B. Costa et al.,[29] that solvatochromic effects can also be ascribed to frictional effects. Generally if all effects are present, then the overall observed shift, $\bar{\nu}_t$, results from the following contributions:

$$\bar{\nu}_t = \bar{\nu}_{gs} + \bar{\nu}_{sp} + \bar{\nu}_{fc} \quad (4)$$

Here, gs refers to general solvatochromic, sp to specific, and fc to mechanical effects.

In the present work, we have investigated the solvatochromic effects that arise when the dyes NR and ZnP are dissolved in a series of non polar and polar solvents and also incorporated in the following rigid media: PS, PVP, SiO_2, and TiO_2. We have found evidence for the coexistence of more than one of those effects, as will be shown in the following sections.

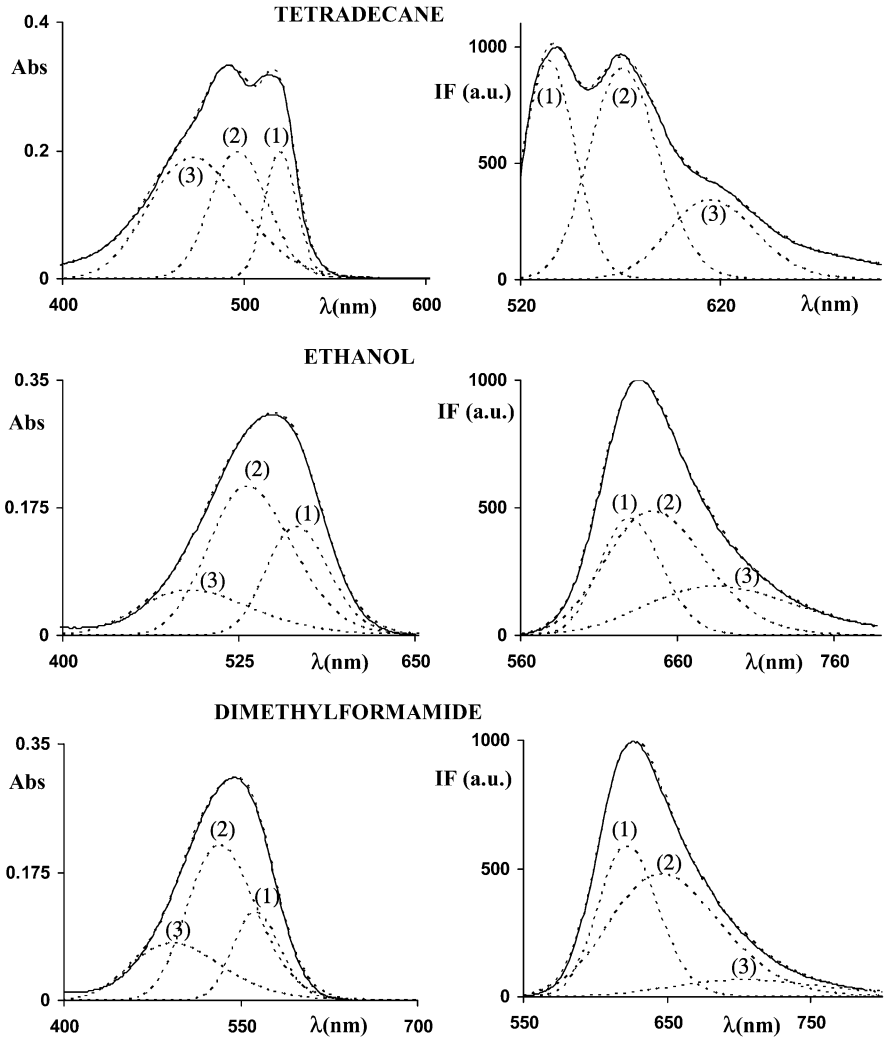

Figure 2. Absorption and emission spectra of NR in tetradecane, ethanol, and dimethylformamide. Shown are the measured spectra (full line) and the calculated ones (broken lines) considering the superimposition of three Gaussian curves.

TABLE 1: Permanent Dipole Moment (μ_g) and Onsager Cavity Radius (R) Obtained for Each Dye in Several Solvents, Using ArgusLab Software[a]

	NR		ZnP		ZnP−Py	
solvent	μ (D)	R (Å)	μ (D)	R (Å)	μ (D)	R (Å)
vacuum	2.74		0.419		6.73	
isooctane	3.03	5.89	0.469	7.47	7.03	7.76
toluene	3.13	5.78	0.486	7.34	7.12	7.63
methanol	3.60	5.90	0.565	7.49	7.50	7.79
ethanol	3.56	5.93	0.560	7.53	7.48	7.82
dimethylformamide	3.80	5.62	0.601	7.13	7.65	7.41
water	3.93	5.51	0.623	6.99	7.74	7.27

[a] The same parameters for the ZnP−Py complex are also shown, where Py stands for pyridine.

Prominent spectral shifts were found for NR, in accordance with previous studies.[9,30] Spectral shifts were also found for ZnP, albeit less pronounced. These results are in agreement with the values obtained for the permanent dipole moment of each dye using the ArgusLab software and shown in Table 1. The relevant properties of the solvents used in this work, refractive index and static dielectric constant, are presented as Supporting Information. In the following sections the shifts observed for each dye are examined in detail in order to characterize the mechanism(s) involved in the present study.

3.1. Solvatochromic Effects in NR. NR is a highly fluorescent dye that displays a spectroscopic behavior largely dependent upon the polarity of the host medium.[9,30] This behavior is due to the intramolecular charge-transfer nature of the electronic states involved in the optical transitions observed.[31] Figure 2, shows the absorption and emission spectra of NR in three of the solvents used in the present work. In agreement with previous authors[9] it was found that the vibrational structure of NR is a prominent feature of the absorption and emission spectra in solvents of low polarity. A significant overlap of absorption and emission spectra is observed in non polar media thus showing that in such solvents the molecular geometry of the dye undergoes minor changes upon excitation. As the solvent polarity is increased pronounced effects are found on both absorption and emission spectra. The results obtained by Dutta et al. on NR in a restricted range of solvents and polar rigid media show a similar trend.[9] The same effect was found by Maroncelli and Fleming[4] on the photophysics of a coumarin dye in several solvents.

To establish the solvatochromic behavior of each vibronic transition, the Gaussian decomposition[31,8] was consistently adopted for the whole range of solvents used throughout instead of the log−normal decomposition[4,5,32] that usually minimizes the number of spectral components, particularly in polar solvents where the structure is lost due to inhomogeneous broadening. However preliminary decompositions of NR spectra (absorption and emission) measured in weakly polar solvents produced the same number of components with either Gaussian or log−

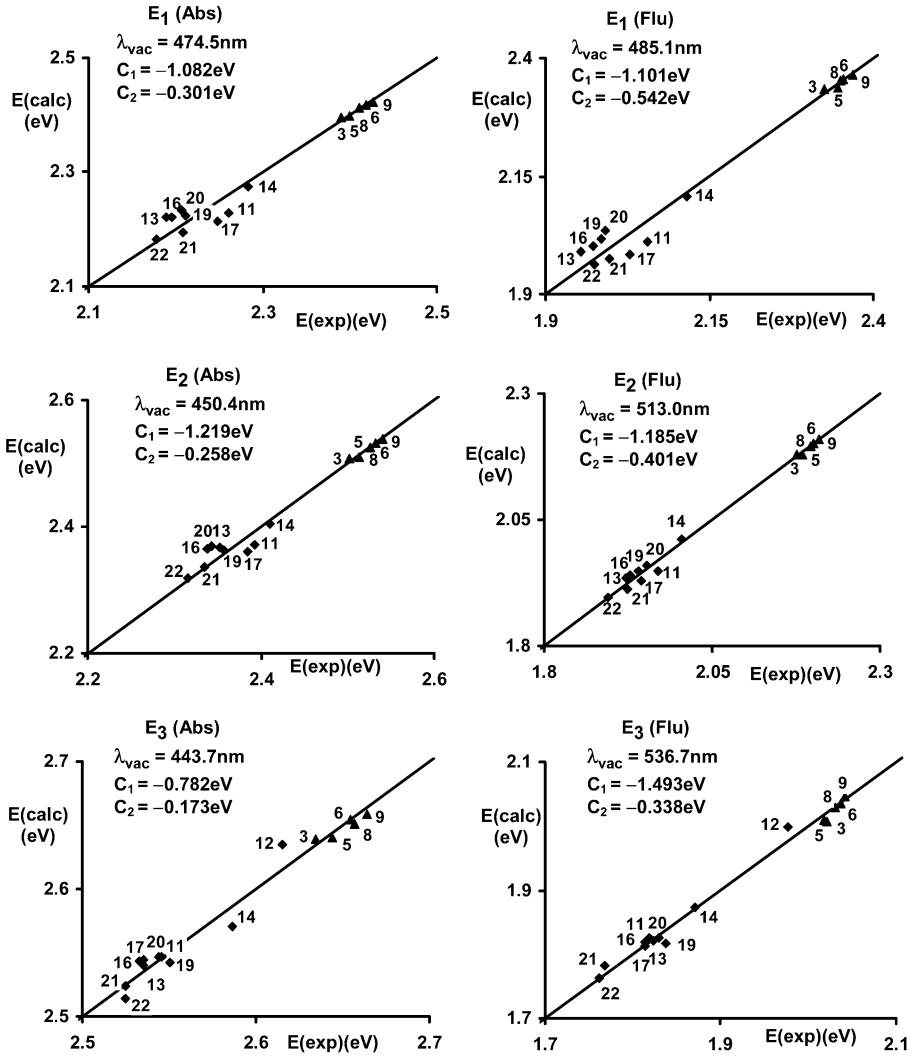

Figure 3. Representation of the calculated energy vs the experimental one for each absorption and emission Gaussian band maximum, according to eqs 1 and 2. Also shown are the best fitted parameters, C_1, C_2, and λ_{vac}. Numbers refer to solvents, given in the Supporting Information.

normal methods. Moreover the Gaussian decomposition is a three parameter function,

$$I(E) = \sum_{i=1}^{n} \frac{A_i}{\sqrt{2\pi}\gamma_i} e^{-(E-E_i)^2/2\gamma_i^2} \qquad (5)$$

whereas the log−normal decomposition is a four-parameter function.[4,32]

The best fits were obtained when each curve was considered the superimposition of three components as shown in Figure 2 for NR in tetradecane, ethanol, and dimethylformamide. All data obtained from this analysis, for the solvents used, are given as Supporting Information. We ascribe these sets of three bands to the following transitions: $S_{0,0} \rightarrow S_{1,0}$, $S_{0,0} \rightarrow S_{1,1}$, and $S_{0,0} \rightarrow S_{1,2}$ in the absorption and the corresponding "mirror image" transitions in the emission. The correlation between observed and calculated frequency shifts for each absorption and emission band, according to eqs 1 and 2 are shown in Figure 3. The fitting parameters are shown in each graph. From such results we conclude that C_1 is always higher than C_2 which indicates that electronic relaxation rather than dipolar relaxation effects dominate the observed solvatochromic shifts. Nevertheless, the magnitude of the values found for C_2 confirm that large changes in the molecule dipole moment upon excitation are observed in the present work, in agreement with previous work.[9,33,34] In fact from the slope of the Mataga−Lippert plot (Figure 4a) a change of dipole moment of $\Delta\mu = 6.1$ D was found by assuming an Onsager cavity radius of $R = 5.8$ Å according to the calculated values presented in Table 1, which are similar to the values used by other workers.[2,9,34,35] It is worth noting that a substantially larger value, $\Delta\mu = 11.6$ D, was found by Dutt et al.[33,35] for NR in media (binary solvents mixtures and viscous media) where the contribution of dielectric friction becomes important.

It is also interesting to note that the width of each band in the emission is narrower than the corresponding absorption band particularly in polar media, as predicted by the model developed by D. V. Matyushov and M. D. Newton.[36] According to this model the line shape will result from the polarizability effect that induces band enlargement and the opposite effect caused by electronic delocalization. The results from the present work are shown in Figure 4b for band 1 of NR. Finally, Table 2 shows time-resolved fluorescence measurements of NR in several solvents and also incorporated into rigid matrixes. In solution all lifetimes are found to be monoexponential, in agreement with previous work.[2,9,17] Most probably the observed lifetime originates from the charge-transfer excited state, as proposed by Ghoneim.[2] The lifetimes observed in the matrixes will be discussed in section 4.1 of this paper.

TABLE 2: Time-Resolved Fluorescence Measurements for NR in Various Solvents and in Rigid Media[a]

solvent/matrix	λ_{exc} (nm)	λ_{em} (nm)	τ_1 (ns)	α_1	τ_2 (ns)	α_2	τ_3 (ns)	α_3	χ^2
tetradecane	500	550	2.76 ± 0.02	1					1.10
toluene	490	>570	4.00 ± 0.02	1					1.04
ethanol	590	650	3.74 ± 0.01	1					1.07
DMF	590	650	4.33 ± 0.02	1					1.11
DMSO	590	650	4.18 ± 0.02	1					1.10
PS	490	>570	4.34 ± 0.01	1					1.18
PVP	490	>570	4.63 ± 0.01	0.93	2.33 ± 0.03	0.07			1.17
sg-SiO_2	490	>570	3.26 ± 0.06	0.50	1.97 ± 0.27	0.50			1.02
sg-TiO_2	490	>570	4.56 ± 0.24	0.02	1.58 ± 0.27	0.17	0.39 ± 0.04	0.81	1.19
sp-TiO_2	490	>570	3.36 ± 0.10	0.02	1.08 ± 0.02	0.23	0.36 ± 0.01	0.75	1.10

[a] The data were analyzed using an equation of the form $I(t) = \sum_i \alpha_i \exp(-t/\tau_i)$. The preexponential factors are given normalized to unity.

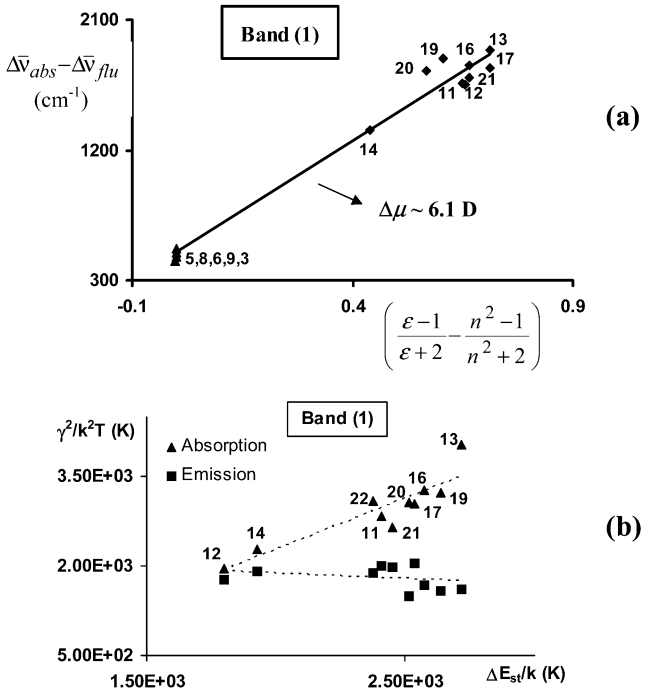

Figure 4. Influence of solvent on band 1 of NR (a) Mataga−Lippert plot showing the large change in dipole moment upon excitation. (b) Absorption and emission bandwidths vs the Stokes shift in polar solvents. Solvent numbers are given in Supporting Information.

3.2. Solvatochromic Effects in ZnP. Part 1. Absorption and emission spectra measured at room temperature were obtained for ZnP in a range of solvents (listed as Supporting Information). The recorded spectra obtained in tetradecane, ethanol. and dimethylformamide are represented in Figure 5, where the influence of the host medium is clearly discernible. Both Q bands display solvent dependence in particular the Q_α in that it becomes more prominent as the solvent polarity increased. The main features in the emission spectra correlate with the corresponding absorption spectra, as shown in the behavior of the Q emission bands. The Soret band also displays a red shift with increasing solvent polarity.

To obtain an accurate description of the solvatochromic effects, both absorption and emission spectra in the Q region were decomposed as a sum of distinct vibronic contributions. Each contribution was assumed to follow a Gaussian profile since all Q bands are highly symmetric.[32] Each spectrum was therefore decomposed according to eq 5. The decomposed absorption and emission spectra are also shown in Figure 5. The ensemble of decomposed spectra show the following features: (a) the Q_α band becomes more prominent on polar solvents in both absorption and emission spectra, the highest band intensity ratio, I_{Q_α}/I_{Q_β}, occurs in DMSO and DMF and the lowest in hexane (see Supporting Information); (b) moreover, the maxima of all Q_α and Q_β bands undergo a systematic red shift as the solvent polarity increases. In general we find that the bandwidth, γ, of the Q absorption bands is higher than the corresponding emission band in agreement with the predictions of the model developed by Matyushov and Newton.[36]

Decomposition of all emission spectra also reveals the presence of a third band, the maximum of which occurs at 611−617 nm and a minor fourth band centered around 700 nm. This fourth band occurs at the onset of the spectral region where the instrumental response is significantly less accurate. Moreover, its intensity and location in the spectrum appear quite independent of the solvent. Under these circumstances we have not investigated in detail the properties of this band in the present work. The new emission band, referred to as NB band, becomes more prominent as solvent polarity increases, the energy of its maximum somewhat dependent upon the nature of the host medium. On the whole, the width of this new band (NB) increases with solvent polarity. The spectral shifts obtained for ZnP in the solvents used throughout show that dye−solvent interaction in this system is less pronounced than the previous NR−solvent system.

It is clear from the work of Nappa and Valentine[37] that a linear correlation between $\Delta\bar{\nu}_{Q_\alpha}$ and $f(n^2)$ could not be unequivocally found for ZnP according to their data, obtained from the measured spectra without spectral decomposition. The work of Renge[38] on the absorption spectra of H_2TPP in polar solvents confirmed the occurrence of a peculiar solvent mechanism to account for the observed shifts in $\Delta\bar{\nu}_{Q_\alpha}$ and $\Delta\bar{\nu}_{Q_\beta}$. The value found for $\Delta\alpha = \alpha_g - \alpha_e$, the difference between ground and excited Franck−Condon state polarizabilities of the porphyrin, was at least an order of magnitude lower than the corresponding values found for polycyclic arenes. Moreover, in view of the symmetry properties of the porphyrin ring the dipole moments of both ground, μ_g, and excited states, μ_e, are expected to be small along with their difference, $\Delta\mu = \mu_g - \mu_e$. The calculated values for μ_g obtained with ArgusLab software can be seen in Table 1, thus confirming this prediction.

In the present work, plots of the observed shifts for the Soret band, Q absorption and emission bands, and the new ZnP emission band, according to the linear terms of eqs 1 and 2, are shown in Figure 6. The respective fitting parameters are also shown in each graph. In all graphs C_1 is higher than C_2, thus indicating that, under our experimental conditions, solvent electronic relaxation prevails over dipolar relaxation effects.

We have further examined the behavior of the Q bands by using eq 3 to estimate $\Delta\mu$. In the present work, from the difference between C_2(Abs) and C_2(Flu), we have obtained $\Delta\mu = 0.6$ D for the Q_α band and $\Delta\mu = 0.7$ D for the Q_β band, by assuming the Onsager radius to be on the order of 7.4 Å

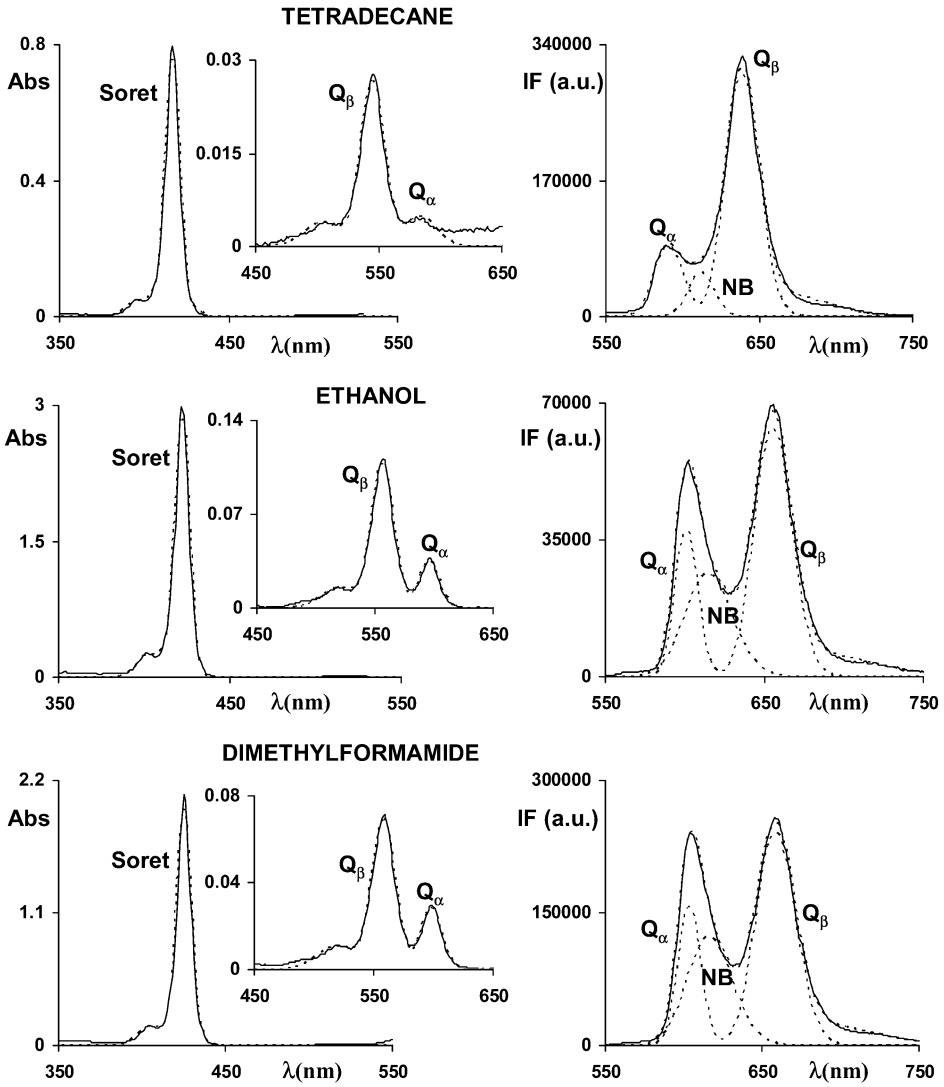

Figure 5. Absorption and emission spectra of ZnP in tetradecane, ethanol, and dimethylformamide. Shown are the measured spectra (full line) and the calculated ones (broken lines) considering the superimposition of Gaussian curves.

according to our calculated values shown in Table 1. Similar R values have also been reported.[38,39]

When eq 2 is applied to the NB band the lowest values of C_1 and C_2 are found. Moreover, the ratio $C_1/C_2 \sim 21$ is the highest. According to these data, we believe that NB emission originates from a different species than the monomeric first excited singlet, ZnP*(S_1). In fact we interpret such emission as originating from exciton coupling between pairs of weakly interacting ZnP molecules, in agreement with the predictions of Tran-Thi et al.[39] based upon the study of solvatochromic effects observed for face to face porphyrin dimers and trimers. We believe that in our case weak coupling is present since the molecular features of the monomer dominate the absorption spectra in all cases. This matter will be further discussed on section 4 where the photophysics of ZnP in rigid matrixes is presented and discussed in conjunction with the results already described.

Part 2. The solution studies on ZnP were further extended to the following system: ZnP and poly(4-vinylpyridine) (PVP) in methanol. Whenever PVP is added to a solution of ZnP in methanol, the Soret band is red shifted as compared with ZnP in pure methanol, as shown in Figure 7, where a red shift of ∼7 nm is also found for the Q bands. Moreover the appearance of a new weak band red-shifted ($\lambda \sim 450$ nm) in relation to the main Soret band can also be found in Figure 7. It is also interesting to note that a new transition red shifted to the main Soret is predicted by the simulation of the absorption spectrum of ZnP−Py, the new species that results from the coordination of one pyridine to the axial ligand of Zn in ZnP. This result was obtained from the ZINDO calculation of the optimized structure (shown in Supporting Information). In view of previous studies[37,40−42] we interpret this behavior as indicative of the formation of a ground-state complex between PVP and ZnP (ZnP−PVP) through the axial coordination of one pyridine group of PVP to the Zn atom of the porphyrin.[41] In this complex PVP acts as donor.[37] This interpretation is further corroborated by the peak ratio I_{Q_α}/I_{Q_β} that changes from 0.80 in ZnP to 1.08 in ZnP−PVP, in agreement with the results of D'Souza et al.[43]

Detailed analysis of the behavior in the Soret region has been performed in the present work according to the following equation:

$$\frac{1}{\dfrac{A(\lambda)}{[\mathrm{ZnP}]_0 l} - \epsilon_\mathrm{P}} = \frac{1}{K[\mathrm{PVP}]_0(\epsilon_\mathrm{C} - \epsilon_\mathrm{P})} + \frac{1}{\epsilon_\mathrm{C} - \epsilon_\mathrm{P}} \qquad (6)$$

Here $A(\lambda)$ = total absorbance at wavelength λ, $[\mathrm{ZnP}]_0$ = total concentration of ZnP, $[\mathrm{PVP}]_0$ = total concentration of PVP, in

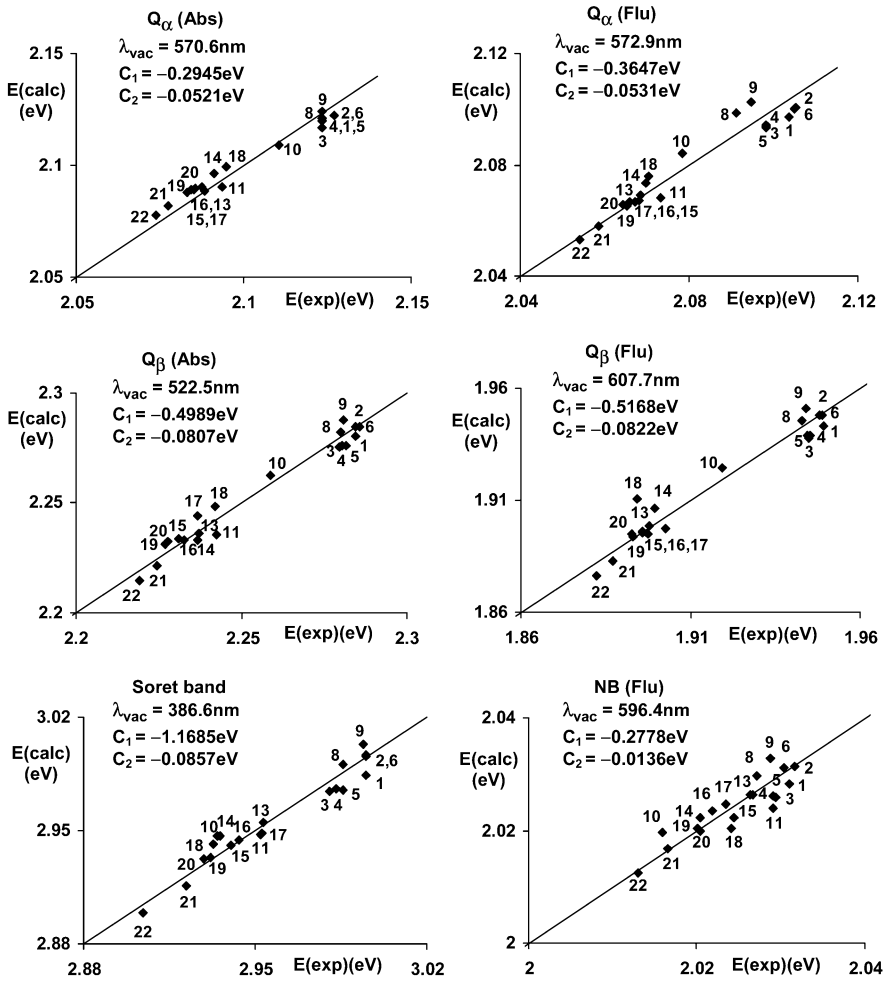

Figure 6. Representation of the calculated energy vs the experimental one for each absorption and emission Gaussian band maximum, according to eqs 1 and 2. Also shown are the best fitted parameters, C_1, C_2, and λ_{vac}. Numbers refer to solvent number given in Supporting Information.

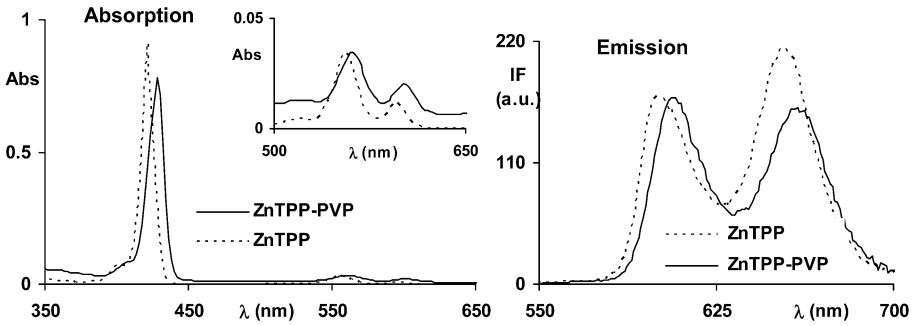

Figure 7. Absorption and emission spectra of ZnP and ZnP−PVP in methanol, showing the typical red shift in the complexed porphyrin.

large excess relative to $[ZnP]_0$, l = optical path length, K = equilibrium constant for ZnP−PVP complex, ϵ_C = extinction coefficient of the complex, and ϵ_P = extinction coefficient of ZnP.

This equation is considered valid under the following experimental conditions: $\epsilon_{PVP} = 0$ and $[PVP]_0 \gg [ZnP]_0$ in the 410−440 nm wavelength region. According to this equation, (a) the ground state of ZnP is either in the monomeric form (ZnP) or associated with PVP in a 1:1 complex, and (b) in the region 410−440 nm, both ZnP and ZnP−PVP absorb. In this work, $[ZnP]_0 = 1.3 \times 10^{-6}$ M and the concentration of PVP is in the range 10^{-3} to 5.8×10^{-2} M, expressed as equivalent vinylpyridine units. The experimental data were fit to eq 6, and the best fit was determined from the least-squares minima by weighting each data point according to its own variance,[44] in view of the fact that the relative errors vary substantially within the range of experimental absorbance data. Figure 8 illustrates the fits obtained for two distinct wavelengths, rewriting eq 6 in the form

$$\frac{A(\lambda)}{[ZnP]_0 l} = \frac{\epsilon_P + \epsilon_C K[PVP]_0}{1 + K[PVP]_0} \qquad (7)$$

According to this method $K = 77 \pm 10$ M^{-1} and the maximum of the Soret band of the complex occurs at $\lambda = 427.0$ nm with an extinction coefficient $\epsilon_C = (5.10 \pm 0.03) \times 10^5$ M^{-1} cm^{-1}. The value found for K in the present work is substantially lower than the value reported by Becker and Hayes,[40] for the same

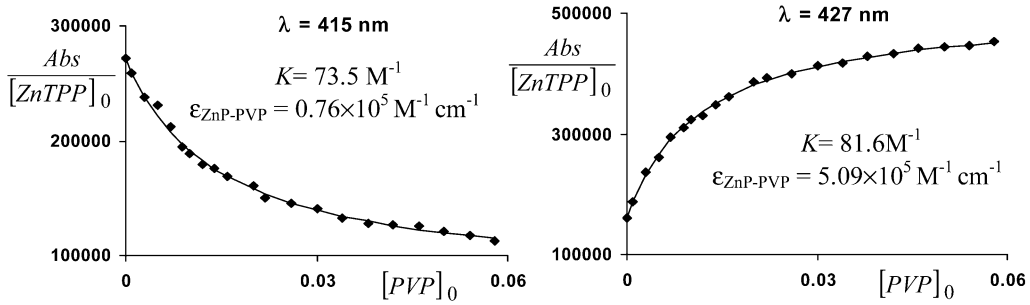

Figure 8. Experimental points and the best fitted curve using weighted least-squares fit according to eq 7. The fitted parameters for each wavelength are also shown.

system but in CH_2Cl_2. In the present study, OH groups of the solvent (methanol) most probably compete with pyridine units of PVP for axial coordination with zinc. The authors believe that the fitting procedure of the spectroscopic data is determinant to the precision of the results, particularly in the case of relatively low values of *K*, as in the present study.

The fluorescence spectra measured in the 550−700 nm also displayed in Figure 7 show that ZnP−PVP is fluorescent with its emission spectra red shifted ∼8 nm relative to monomeric ZnP in methanol. The emission spectra obtained upon excitation at different wavelengths of the absorption spectra were analyzed by assuming that the first singlet state of the monomer and the complex follow identical routes:

$$\mathrm{ZnP} + \mathrm{PVP} \xrightarrow{K} \mathrm{ZnP{-}PVP}$$

$$\mathrm{ZnP} + h\nu \rightarrow \mathrm{ZnP}^*$$

$$\mathrm{ZnP}^* \xrightarrow{k_{NR}} \mathrm{ZnP}$$

$$\mathrm{ZnP}^* \xrightarrow{k_F} \mathrm{ZnP} + h\nu_F$$

$$\mathrm{ZnP{-}PVP} + h\nu \rightarrow (\mathrm{ZnP{-}PVP})^*$$

$$(\mathrm{ZnP{-}PVP})^* \xrightarrow{k'_{NR}} (\mathrm{ZnP{-}PVP})$$

$$(\mathrm{ZnP{-}PVP})^* \xrightarrow{k'_F} (\mathrm{ZnP{-}PVP}) + h\nu'_F$$

According to this scheme, under steady-state conditions the following equation holds:

$$\frac{\phi}{\phi_0\delta} = 1 + \frac{k'_F\tau'}{k_F\tau}\left(\frac{1-\delta}{\delta}\right) \qquad (8)$$

ϕ and ϕ_0 are the fluorescence quantum yields of the system in the presence and in absence of PVP, τ and τ' are the lifetimes of ZnP and ZnP−PVP, respectively, and δ is the fraction of the exciting beam that is absorbed by free ZnP. Equation 8 enables us to obtain the relationship between the fluorescence quantum yields of the two species, ZnP−PVP and ZnP. The results are shown in Figure 9, and under the experimental conditions described, it was found that $k'_F\tau'/k_F\tau = 1$ thus confirming that the photophysics of ZnP in methanol is not significantly affected by the axial coordination of the pyridine units of PVP to the central zinc atom.

The solvatochromic effects observed on the Q bands of ZnP−PVP absorption and emission can be resolved into two components:

$$\bar{\nu}_t = \bar{\nu}_{gs} + \bar{\nu}_{sp}$$

In fact, for example for Q_α emission band in methanol,

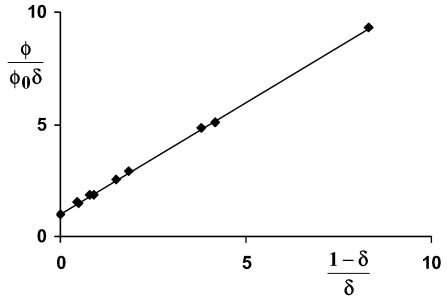

Figure 9. Experimental results according to eq 8, showing that $k'_F\tau'/k_F\tau \approx 1$.

$\bar{\nu}_{sp} = 192\ \mathrm{cm}^{-1}$ is ascribed to the formation of the complex, as previously described, whereas $\bar{\nu}_{gs} = 799.8\ \mathrm{cm}^{-1}$ is identical to the spectral shift reported in Part 1 for ZnP in the same solvent, but in the absence of PVP.

4. Photophysics of the Dye-matrix Systems

4.1. Nile Red in Rigid Media. We now report on the photophysics of NR when incorporated into the following matrixes: polystyrene (PS), poly(4-vinylpyridine) (PVP), SiO_2 prepared by sol−gel (sg-SiO_2), and TiO_2, prepared by sol−gel (sg-TiO_2) and by magnetron sputtering (sp-TiO_2). All samples were prepared as thin films, according to the experimental details described in section 2.

Figure 10 shows the absorption and emission spectra of NR in PS and PVP. Some residual vibronic structure can be seen in the absorption and emission of NR−PS system whereas the spectrum of NR−PVP shows no structure, as expected since PVP is a more polar environment than PS. According to Table 2, the time-resolved emission of NR in PS is monoexponential, with a fluorescence lifetime $\tau = 4.34$ ns, whereas the decay measured in PVP could be resolved into two components, $\tau_1 = 4.63$ ns and $\tau_2 = 2.33$ ns. The long-lived component is the largely dominant one, thus showing that PVP is probed by NR as an almost homogeneous and rather polar environment. Also shown in Figure 10 is the emission spectrum of NR when incorporated into SiO_2 and TiO_2. The localization and shape of the bands confirm that NR emission in both sg-SiO_2 and sp-TiO_2 originates from polar environments. The peak maximum occurs at 639 nm in sg-SiO_2 and 626 nm in sp-TiO_2, thus suggesting that the silica film is a more polar environment.

The fluorescence decay of NR incorporated into sg-SiO_2 could also be resolved into two components, $\tau_1 = 3.26$ ns and $\tau_2 = 1.97$ ns, with identical preexponential factors. The emission decay of NR when encapsulated into sp-TiO_2 is also dominated by two fast components 0.36 and 1.08 ns. A minor longer lived component (3.36 ns) was also found, thus confirming that dye-matrix interaction must control the kinetics of NR fluorescence

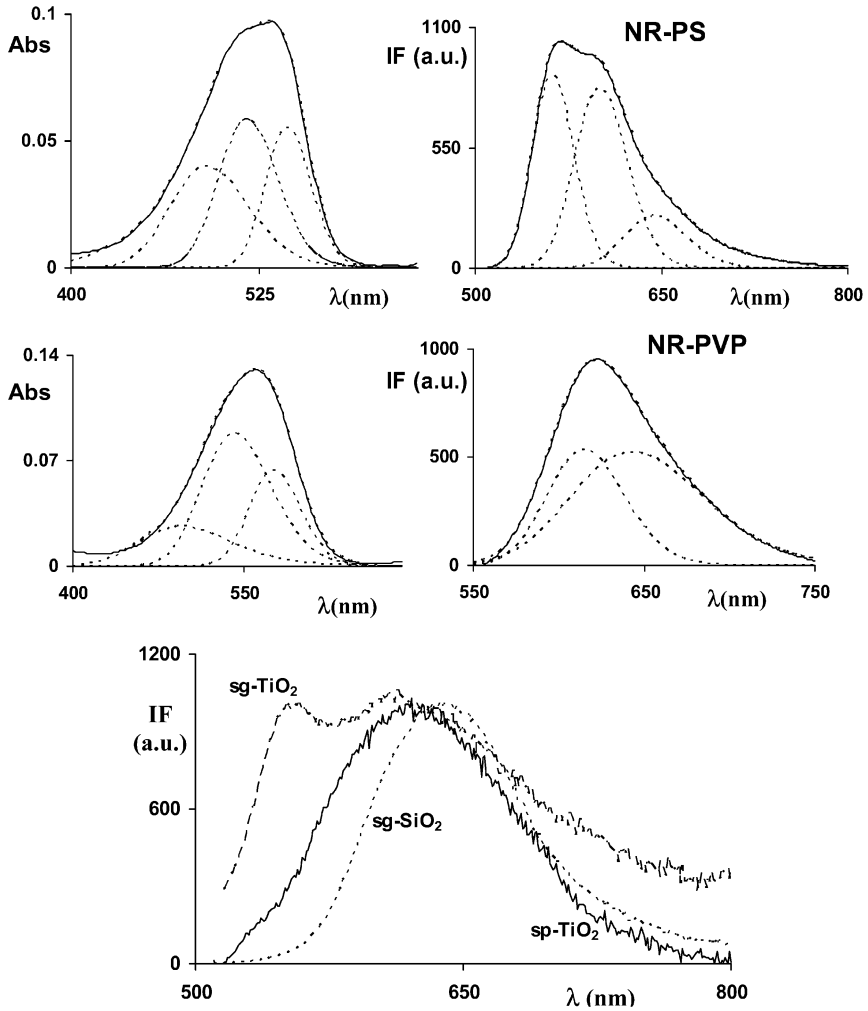

Figure 10. Spectrum for nile red incorporated in different rigid matrixes, showing the absorption and emission spectra in polymeric matrixes of PS and PVP. The measured spectra (full line) and the calculated ones (broken lines) considering the superimposition of three Gaussian curves are given. The emission spectra are also shown for NR in the SiO_2 and TiO_2 matrixes.

decay. When NR is incorporated into sg-TiO_2, a more complex emission is observed with two major bands at 555 and 613 nm. According to the spectra shown in Figure 10, the occurrence of these bands suggests that sg-TiO_2 behaves as a less polar environment to NR than sp-TiO_2. Fluorescence decays from NR in sg-TiO_2 were resolved into three components, a minor longer lived, $\tau_1 = 4.56$ ns, and two short-lived components, $\tau_2 = 1.58$ ns and $\tau_3 = 0.39$ ns, suggesting that NR most probably interacts significantly with TiO_2, in view of the fact that the fast components are a dominant feature of the emission decay.

To correlate the spectral shifts described in this section with the results of section 3.1, the energy shifts of the most intense band of the measured emissions of NR in solution where plotted according to eq 2. This plot is shown in Figure 11. The experimental shifts observed for the rigid media are plotted on the best fit line obtained from the spectral shifts in solution. In this way it was possible to estimate the effective local dielectric constants, ϵ_{eff}, probed by NR in the following media, PS, PVP, SiO_2, and TiO_2, from the corresponding values of the calculated spectral shifts, E_{calcd}. The inset of Figure 11 shows the estimated values of the effective dielectric constants probed by NR in each medium. The effective values of the refractive index, n_{eff}, were obtained from the detailed analysis of the transmittance spectra of each matrix, as previously reported[20] and were found to be always smaller than the bulk ones, due to the porosity of the films.

It is interesting to note the agreement between ϵ_{eff} obtained for PS and PVP and the literature values, 2.5 for PS[45] and 10.5 for vinylpyridine.[46] The values of ϵ_{eff} thus obtained for the different media reveal the following features: (a) the polar environment probed by NR in PVP, as due to the presence of the pyridine units of PVP copolymer; (b) the high polarity of SiO_2 sol−gel thin films as compared with $n = 1.54$ and $\epsilon = 3.8$ for bulk SiO_2[46] (which is due to the porous structure of the sol−gel that favors solvent retention within the matrix pores, as previously reported by several authors);[17,47] (c) the optically homogeneous sp-TiO_2 films displaying volumetric void fractions, f_v, on the order of 13% and an average pore radius on the order of 20 Å.[18,20] These relatively dense matrixes display effective dielectric constants on the order of 16.3 due to the polar hydroxyl groups that are abundant on the titania surface;[48] the presence of adsorbed water molecules within the pores is also to be expected thus explaining the relatively high ϵ_{eff} found in this film as compared with $\epsilon = 6.0$ for bulk TiO_2 (anatase).[49] On the other hand sg-TiO_2 matrixes are substantially more porous with void fractions on the order of 54%[20] and effective dielectric constant lower than the sputtered matrixes.

4.2. ZnP in Rigid Media. The behavior of ZnP emission when incorporated into the following matrixes: PS, PVP, sg-SiO_2, and sp-TiO_2 is examined in this section. From previous studies,[20] the authors have found that, in the ZnP-sp-TiO_2 system, the porphyrin becomes "anchored" onto the surface of

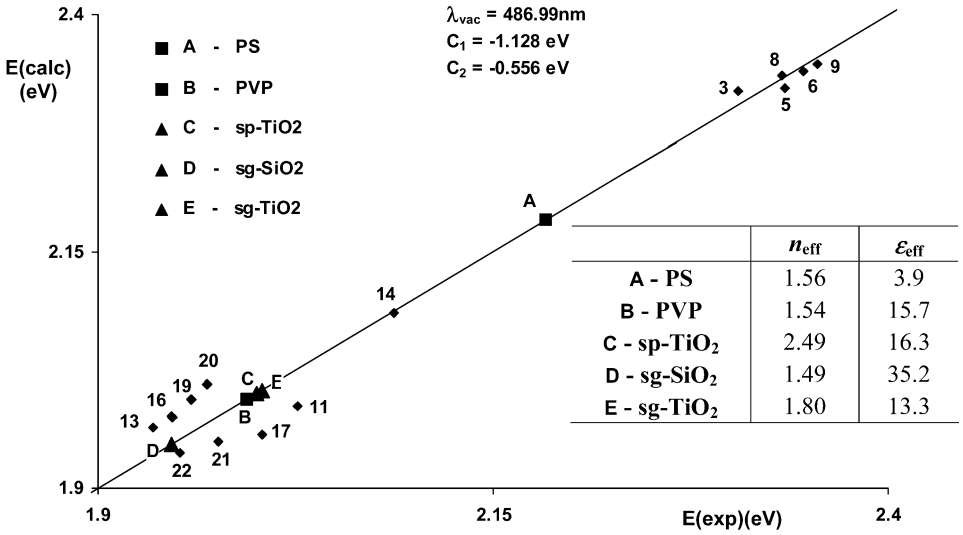

	n_{eff}	ε_{eff}
A - PS	1.56	3.9
B - PVP	1.54	15.7
C - sp-TiO_2	2.49	16.3
D - sg-SiO_2	1.49	35.2
E - sg-TiO_2	1.80	13.3

Figure 11. Representation of the calculated energy according to eq 2 vs the measured one for the most intense emission band of NR in different solvents. Plotted on the best fit line obtained from the solution measurements, are the measured energy maxima for the rigid media. Numbers refer to solvent number in Supporting Information.

the semiconductor as a monomer or in the form of aggregates. These aggregates are fluorescent and their presence was also detected from the detailed analysis of the Soret band. In the present work these results are revisited and further examined in the light of the occurrence of the new band (NB) in the solution studies reported in section 3.2. In fact it is assumed that this NB occurs as the result of a weak excitonic coupling between pairs of porphyrin molecules, in solution. The decomposed Soret band found for ZnP-sp-TiO_2, shown in Figure 5 of ref 20, is now interpreted as evidence for a stronger excitonic coupling between ZnP molecules when assisted by the TiO_2 matrix. This argument is further corroborated by the observation of aggregate emission. In fact, as predicted by Kasha's exciton theory,[50,51] if the geometry of the excitonic pair is like the one shown in Figure 12, then the exciton singlet splitting energy will depend on θ according to

$$\Delta E = 2\left(\frac{\mu^2}{R^3}\right)(1 + \cos^2\theta) \qquad (9)$$

where: μ is the transition dipolar moment for the singlet−singlet transition in the monomer, R is the center to center distance between molecules and θ is the angle made by the polarization axes with the line of the molecular centers.

According to this energy diagram, both blue-shifted and red-shifted absorption bands are to be expected. However, internal conversion from the upper to the lower excitonic state can explain the observation of the red shifted emission solely from the aggregate. Application of Kasha's theory to the NB emission in methanol (section 3.2), under the assumption that this band corresponds to the Q_α transition in the monomer, allows the following parameters to be calculated:

$$\Delta E = 0.088 \text{ eV } (720 \text{ cm}^{-1})$$
$$R = 3.1 \text{ Å}, \quad \text{for } \theta = 90°$$
$$R = 3.9 \text{ Å}, \quad \text{for } \theta = 0°$$

In these calculations it was assumed that for the Q_α emission band $\mu = 1.44$ D, obtained from the absorption spectrum. Most probably, a hole range of intermediate configurations occur since the two molecules are not chemically linked, therefore the two configurations, $\theta = 0°$ and $\theta = 90°$, would be limiting cases of

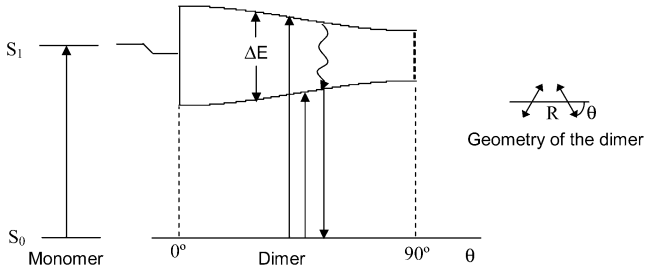

Figure 12. Exciton singlet splitting for dimers with nonparallel transition moments, as a function of θ.

the distribution of real "face to face" configurations. A similar type of excited-state pairs (dimers) was reported by Nakashima el al.[52] for covalently linked zinc porphyrins; these authors found evidence for $\pi-\pi$ interaction in the S_1 state.

Analysis of the splitting found in the Soret band of ZnP-sp-TiO_2, considering the decomposition shown in Figure 5 of ref 20, reveals a stronger exciton coupling energy as would be expected; in fact in this system

$$\Delta E = 0.166 \text{ eV } (1340 \text{ cm}^{-1}), \quad \text{with } \mu = 2.98 \text{ D}.$$

Under these conditions the following values of R are found:

$$R = 4.1 \text{ Å}, \quad \text{for } \theta = 90°$$
$$R = 5.1 \text{ Å}, \quad \text{for } \theta = 0°$$

Examination of the so-called aggregate emission[20] shown in Figure 13 reveals the following features: (a) the spectrum can be resolved into three components centered at the following energies $E_3 = 1.86$ eV (668.2 nm), $E_4 = 1.81$ eV (686.6 nm), and $E_5 = 1.73$ eV (715.6 nm). The bands pertaining to the monomer S_1 emission are E_1 (Q_α) = 2.07 eV (601.3 nm) and E_2 (Q_β) = 1.90 eV (653.5 nm). The large spectral shifts observed in the emission, as compared with the Soret band spectral shifts, can only be in agreement with the corresponding exciton coupling energy found in the absorption spectrum if band E_3 (Q'_β) is correlated with E_2 (Q_β) emission rather than with E_1 (Q_α). To explain this behavior, it is assumed that the appropriate potential energy surface diagram will be qualitatively described as shown in Figure 13. Under this assumption

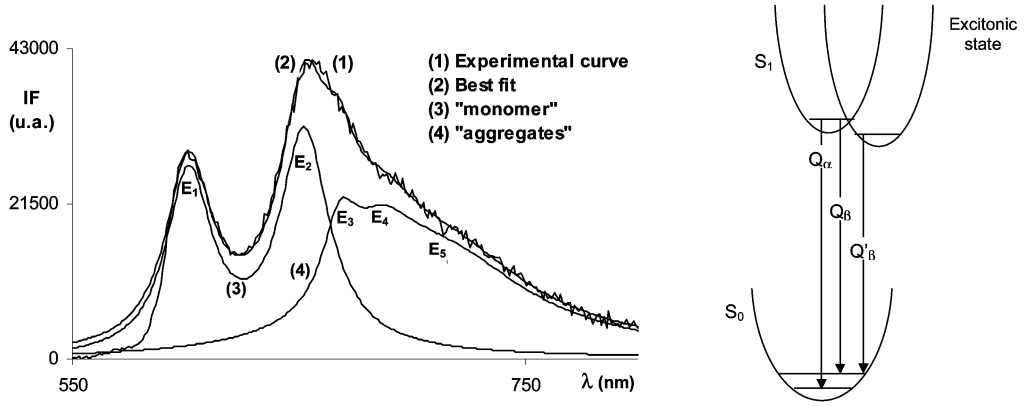

Figure 13. ZnP-sp-TiO_2 matrix, showing measured and calculated fluorescence spectra displaying two emissions, one ascribed to the monomer and the other to "aggregates", along with the related schematic potential energy surface diagram.

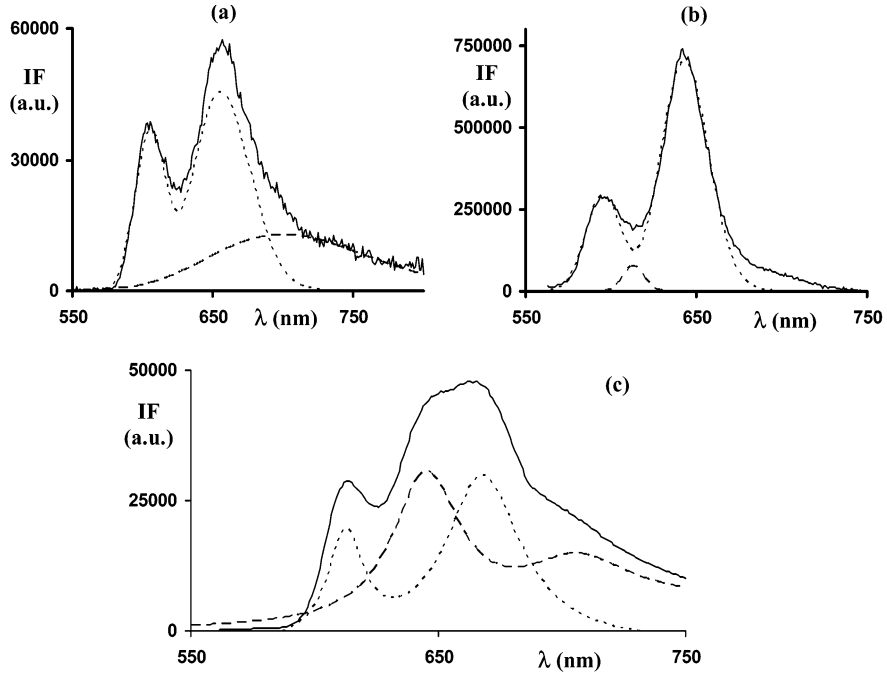

Figure 14. Fluorescence spectra and related decomposition of ZnP in different matrixes, (a) ZnP-sg-SiO_2, (b) ZnP−PS, and (c) ZnP−PVP.

the following parameters

$$\Delta E\ (Q_\beta) = 0.1\ \text{eV}\ (808\ \text{cm}^{-1})$$

$$R = 3.9\ \text{Å}, \quad \text{for}\ \theta = 90°$$

$$R = 4.9\ \text{Å}, \quad \text{for}\ \theta = 0°$$

are obtained. From the analysis of the absorption and emission parameters of ZnP incorporated into sp-TiO_2[20] it was found that $\mu = 2.21$ D.

The occurrence of bands E_4 and E_5 can also be accounted for if they are considered to originate from aggregates of more than two ZnP molecules. In fact the theory was further extended to aggregates of $N > 2$ molecular units.[51] If this methodology is applied to the E_4 band R becomes 4.2 ($\theta = 90°$) and 5.3 Å ($\theta = 0°$) in the limit of $N \rightarrow \infty$. The last band, E_5, was not examined in detail in view of the fact that it occurs at the spectral region where instrumental response is significantly less accurate. The relevant parameters on the excitonic coupling effects on ZnP photophysics are summarized in Table 3.

Emission from the ZnP−SiO_2 system, shown in Figure 14a, is similar to the monomeric emission found in TiO_2 except that the Q_α and Q_β bandwidths are now larger than ZnP−TiO_2 monomer fluorescence. This behavior suggests a significant degree of chemical disorder in the host medium, in conjunction with absence of any significant interaction between the porphyrin and the host matrix. A very broad band centered at ~700 nm was found but not investigated, in view of the poor instrumental resolution in this spectral region.

TABLE 3: Parameters Associated with Exciton Coupling[a]

system	band	ΔE (cm^{-1})	μ (D)	$R(\theta=90°)$ (Å)	$R(\theta=0°)$ (Å)
ZnP/MeOH	Q_α^{em}	720	1.44	3.1	3.9
ZnP/PS	Q_α^{em}	970	1.45	2.8	3.5
ZnP/sp-TiO_2	Soret	1340	2.98	4.1	5.1
	Q_β^{em}	808	2.21	3.9	4.9

[a] μ values were estimated from absorption spectra and emission lifetimes; R values were calculated from eq 9.

Fluorescence from ZnP−PS, shown in Figure 14b, also displays the NB emission detected in solution. The parameters associated with excitonic coupling in PS are also shown in Table 3. The emission ascribed to monomeric ZnP shows the characteristics of a medium of low polarity in that the ratio $I_{Q\alpha}/I_{Q\beta} = 0.15$ behaves in a similar way to the studies reported in section 3.1. The spectral shift measured for the Q_α band is

TABLE 4: Calculated General Solvatochromic Shift[a] and Specific Shift, Observed in the Q_α Emission Band and also Experimental Shifts from the Measured Fluorescence Spectra[b]

system	n_{eff}	ϵ_{eff}	$\Delta\bar{\nu}_{expt}$ (cm^{-1})	$(\Delta\bar{\nu}_{calcd})_{gs}$ (cm^{-1})	$(\Delta\bar{\nu})_{sp}$ (cm^{-1})
ZnP/MeOH	1.33	33.6	802	800	
ZnP/PVP-MeOH	1.33	33.6	994	800	192
ZnP/PVP	1.54	15.7	1115	922	189
ZnP/PS	1.56	2.5	722	678	
ZnP/sp-TiO_2	2.49	16.3	830	1225	

[a] Using eq 2 and the fitted parameters, C_1, C_2, and λ_{vac}, shown in Figure 6. [b] n_{eff} and ϵ_{eff} were picked from the Supporting Information.

in agreement with the calculated one from the general solvatochromic effects, as shown in Table 4. The fluorescence decay from ZnP−PS could be resolved into three components, $\tau_1 = 0.7$ ns, $\tau_2 = 1.9$ ns, and $\tau_3 = 3.5$ ns with the following relative abundances 27%, 62% and 11%, respectively. The fastest component is attributed to the excitonic emission whereas the 1.9 ns decay most probably originates from the S_1 state of monomeric ZnP. The slowest component is ascribed to ZnP monomer units located in a more rigid local environment within the polymeric network.

It is important to note that, for the ZnP-sp-TiO_2 sample, the calculated value of $\Delta\bar{\nu}_{gs} = 1225$ cm^{-1} shown in Table 4 is significantly higher that 830 cm^{-1}, the experimental one. This difference suggests that ZnP probes a local refractive index lower than the average effective value of 2.49. This is not unexpected since ZnP is anchored in the matrix-pore interface where the local TiO_2 density is lower than the average of the film. In fact if a local refractive index of 1.4 is assumed the calculated $\Delta\bar{\nu}$ becomes identical to the experimental one.

Finally it should be noted that the previously reported emission from the ZnP−PVP system is now interpreted in the light of the solvatochromic effects reported in the present work. It is interesting to note that, in this system, the measured spectral shifts of Q_α for the so-called species I,[20] shown in Figure 14c, result from the combination of two effects: (a) specific interaction between the zinc porphyrin atom and the pyridine groups of PVP, $\Delta\bar{\nu}_{sp} = 189$ cm^{-1}, and (b) general solvatochromic effects, $\Delta\bar{\nu}_{gs} = 922$ cm^{-1}, when considering $\epsilon_{eff} \sim 15.7$ D, as obtained from the studies reported in section 4.1 for NR−PVP. These data are also shown in Table 4. Emission II is significantly red shifted with respect to emission I. The occurrence of both emissions (I and II) suggest the following mechanism: part of the excited molecules may decay directly to the ground state whereas other molecules may relax to a more polar metastable state from which emission II will then occur. This explanation is supported by the fact that excitation spectra measured at 612, 645, 668, and 710 nm were identical, which indicates that both emissions originate from the excitation of the same ground-state molecular species.

5. Conclusion

In this work, we have studied the solvatochromic shifts in the absorption and emission spectra of NR and ZnP in a great diversity of solvents from polar to apolar. From the experimental and calculated shifts we have estimated the change in dipole moments upon excitation to be $\Delta\mu = 6.1$ D for NR and $\Delta\mu = 0.60$ D for ZnP. From the ZINDO calculation performed using a PM3 optimized structure, we have simulated the absorption spectra and calculated the permanent dipole moments (μ) and the Onsager cavity radius (R) of the dyes. For NR, μ ranges from 2.74 D in a vacuum to 3.93 D in water and $R \sim 5.8$ Å. For ZnP, $\mu = 0.42$ D in a vacuum and 0.62 D in water and $R \sim 7.4$ Å. The general solvatochromic effects were found to be predominantly ascribed to electronic relaxation in both dyes. We have also performed a spectroscopic characterization of the ZnP−PVP system, where a ground-state interaction between the Zn atom of the porphyrin molecule and the pyridine was observed with $K \sim 77$ M^{-1}. In the ZnP emission spectra in solution we were able to observe a new band (NB) that was interpreted as resulting from an excitonic coupling between interacting ZnP* molecules. Using Kasha's theory and the measured excitonic splitting we have calculated the center to center distance of interacting molecules in methanol to be in the range 3.1 ($\theta = 90°$) to 3.9 Å ($\theta = 0°$).

We have also studied the photophysics of the dyes when incorporated in rigid media. NR in PS, PVP, SiO_2, and TiO_2 probes local polarities, and it was possible for us to estimate the effective dielectric constants of the matrixes. ZnP emission in PS and TiO_2 again reveals an excitonic coupling between porphyrin molecules. In PS, the center to center distance was somewhat lower than in solution while in sp-TiO_2 a higher value was obtained. ZnP emission in SiO_2 resembles that of a monomeric species in a weakly polar medium and the ZnP−PVP emission spectrum was interpreted as originating from two distinct excited states with different polarities.

Supporting Information Available: Tables giving refractive index and static dielectric constant data, fitted parameters according to eq 5 for decomposition of absorption and emission spectra of NR in several solvents, and decomposition data for spectra of ZnP in several solvents according to eq 5 and a figure showing simulated (ZINDO) absorption spectra of ZnP, ZnP−Py, and ZnP−PVP. This material is available free of charge via the Internet at http://pubs.acs.org.

References and Notes

(1) Meyer, M.; Mialocq, J. C. *Opt. Commun.* **1987**, *64*, 264.
(2) Ghoneim, N. *Spectrochim. Acta Part A* **2000**, *56*, 1003.
(3) Renge, I. *J. Phys. Chem. A* **2000**, *104*, 7452.
(4) Maroncelli, M; Fleming, G. R. *J. Chem. Phys.* **1987**, *86*, 6221.
(5) Krishna, M. M. G. *J. Phys. Chem. A* **1999**, *103*, 3589.
(6) Hungerford, G.; Castanheira, E.; Oliveira, M. E.; Miguel, M. G.; Burrows, H. *J. Phys. Chem. B.* **2002**, *106*, 4061.
(7) Hungerford, G.; Pereira, M. R.; Ferreira, J. A.; Viseu, T. M. R.; Coelho, A. F.; Ferreira, M. I. C. *J. Fluorescence* **2002**, *12*, 395.
(8) Innocenzi, P.; Kozuka, H.; Yoko, T. *J. Non-Cryst. Solids* **1996**, *201*, 26.
(9) Dutta, A. K.; Kamada, K.; Ohta, K. *J. Photochem. Photobiol. A: Chem.* **1996**, *93*, 57.
(10) Lakowicz, J. R. *Topics in Fluorescence Spectroscopy, Vol. IV−Biochemical Applications*; Plenum Press, New York, 1991.
(11) www.cci.virginia.edu.
(12) Periasamy, A. *Methods in Cellular Imaging*; Oxford University Press: New York, 2001.
(13) Andersson-Engels, S.; Kaschke, M. F., Eds. Photon Migration, Optical Coherence Tomography and Microcopy. In *Progress in Biomedical Optics and Imaging*, Vol. 2, no. 31, Proceedings of SPIE (June 2001); SPIE: Bellingham, WA, 2001.
(14) Rettig, W.; Strehmel, B.; Schrader, S.; Seifert, H. *Applied Fluorescence in Chemistry, Biology and Medicine*, Springer-Verlag: Berlin, 1999.
(15) Valeur, B.; Brochon, J.-C., Eds.; *New Trends in Fluorescence Spectroscopy: Applications to Chemical and Life Sciences*, Springer Series on Fluorescence 1; Springer-Verlag: Berlin, 2001.
(16) Lakowicz, J. R. *Principles of Fluorescence Spectroscopy*; Plenum Press: New York, 1986.
(17) Hungerford, G.; Ferreira, J. A. *J. Lumin.* **2001**, *93*, 155.
(18) Viseu, T. M. R.; Almeida, B.; Stchakovsky, M.; Drevillon, B.; Ferreira, M. I. C.; Sousa, J. B. *Thin Solid Films* **2001**, *401*, 216.
(19) Hungerford, G.; Suhling, K.; Ferreira, J. A. *J. Photochem. Photobiol. A* **1999**, *129*, 71.
(20) Viseu, T. M. R.; Hungerford, G.; Ferreira, M. I. C. *J. Phys. Chem. B* **2002**, *106*, 1853.
(21) Webman, I.; Jortner, J.; Cohen, M. H. *Phys. Rev. B* **1977**, *15*, 5712.

(22) Reisfeld, R. *J. Non Cryst. Solids* **1990**, *121*, 254.
(23) Zerner, M. C.; Loew, G. H.; Kirchner, R. F.; Mueller-Westerhoff, U. T. *J. Am. Chem. Soc.* **1980**, *102*, 589.
(24) Zerner, M. C. Semiempirical Molecular Orbital Methods. In *Reviews in Computational Chemistry II*; Lipkowitz, K. B., Boyd, D. B., Eds.; VCH Publishers Inc.: Weinheim, Germany, 1991; Chapter 8.
(25) Mataga, N.; Kubota, T. *Molecular Interactions and Molecular Spectra*; Marcel Dekker, Inc.: New York, 1970; Chapter 8.
(26) Kolling, O. W. *J. Phys. Chem.* **1989**, *93*, 3436.
(27) Kairutdinov, R. F.; Serpone, N. *J. Phys. Chem.* **1995**, *99*, 11952.
(28) Zaitzeva, S. V.; Zdanovich, S. A.; Ageeva, T. A.; Ocheretovi, A. S.; Golubchikov, O. A. *Molecules* **2000**, *5*, 786.
(29) Ferreira, J. A. B.; Costa, S. M. B.; Ferreira, L. F. V. *J. Phys. Chem. A* **2000**, *104*, 11909.
(30) Deye, J. F.; Berger, T. A. *Anal. Chem.* **1990**, *62*, 615.
(31) Boldrini, B.; Cavalli, E.; Painelli, A.; Terenziani, F. *J. Phys. Chem. A* **2002**, *106*, 6286.
(32) Siano, D. B.; Metzler, D. E. *J. Chem. Phys.* **1969**, *51*, 1856.
(33) Dutt, G. B.; Doraiswamy, S.; Periasamy, N. *J. Chem. Phys.* **1991**, *94*, 5360.
(34) Sarkar, N.; Das, K.; Nath, D. N.; Bhattacharya, K. *Langmuir* **1994**, *10*, 326.
(35) Dutt, G. B.; Doraiswamy, S.; Periasamy, N.; Venkataraman, B. *J. Chem. Phys.* **1990**, *93*, 8498.
(36) Matyushov, D. V.; Newton, M. D. *J. Phys. Chem. A* **2001**, *105*, 8516.
(37) Nappa, M.; Valentine, J. S. *J. Am. Chem. Soc.* **1978**, *100*, 5075.
(38) Renge, I. *Chem. Phys. Lett.* **1991**, *185*, 231.
(39) Tran-Thi, T. H.; Lipskier, J. F.; Maillard, P.; Momenteau, M.; Lopez-Castillo, J.-M.; Jay-Gerin, J.-P. *J. Phys. Chem.* **1992**, *96*, 1073.
(40) Becker, D. S.; Hayes, R. G. *Inorg. Chem.* **1983**, *22*, 3050.
(41) Vogel, G. C.; Stahlbush, J. R. *Inorg. Chem.* **1977**, *16*, 950.
(42) Ohno, O.; Kaizu, Y. Kobayashi, H. *J. Chem. Phys.* **1985**, *82*, 1779.
(43) D'Souza, F.; Hsieh, Y−Y.; Deviprasad, G. R. *Inorg. Chem.* **1996**, *35*, 5747.
(44) Bevington, P. R. *Data Reduction and Error Analysis for the Physical Sciences*; McGraw-Hill Inc.: New York, 1969; Chapter 6.
(45) Brandrup, J.; Immergut, E. H. *Polymer Handbook*; John Wiley & Sons Inc.: New York, 1989.
(46) Lide, D. R. *Handbook of Chemistry and Physics*; CRC Press, 83th edition.
(47) Delmarre, D.; Veret-Lemarinier, A.-V.; Bied-Charreton, C. *J. Lumin.* **1999**, *82*, 57.
(48) Kumar, P. M.; Badrinarayanan, S.; Sastry, M. *Thin Solid Films* **2000**, *358*, 122.
(49) Mo, S.-D.; Ching, W. Y. *Phys. Rev. B* **1995**, *51*, 13023.
(50) Kasha, M.; Rawls, H. R.; El-Bayoumi, M. A. *Pure Appl. Chem.* **1965**, *11*, 371.
(51) McRae, E. G.; Kasha, M. *J. Chem. Phys.* **1958**, *28*, 721.
(52) Nakashima, S.; Tanigushi, S.; Okada, T.; Osuka, A.; Mizutani, Y.; Kitagawa, T. *J. Phys. Chem. A* **1999**, *103*, 9184.